Progress In Electromagnetics Research C, Vol. 101, 133–146, 2020

High-Gain and Circularly Polarized Fractal Antenna Array for Dedicated Short Range Communication Systems

Deven G. Patanvariya*, Anirban Chatterjee, and Kalyan Kola

Abstract—In this paper, a low-profile fractal antenna and its array for DSRC-band applications have been proposed. The proposed single element is a newly designed fractal antenna which is right-handed circularly polarized (RHCP) and derived from the Koch-snowflake 1st-iteration. Moreover, a diagonal slot defect in the ground plane has been implemented for resonating the structure at the desired frequency and, to get a low cross-polarization over the operating frequency. The compact feed-network of the array is designed using a Wilkinson power-divider. A single element and a 4×1 antenna array are designed, prototyped, and verified. The antenna array is designed by a single-layer microstrip structure with a compact size of $151.70 \times 43.50\,\text{mm}^2$. According to the experimental results, the single element and the antenna array have S_{11} of $-15.27\,\text{dB}$ and $-13.95\,\text{dB}$, and RHCP gain of 6.14 dBic and 11.98 dBic, respectively. Moreover, the computed radiation efficiencies of single element and array are 78.17% and 71.50%, respectively, while CP bandwidths of single element and array are 49.00 MHz and 58.00 MHz, respectively. The performance of the proposed RHCP antenna is suitable for the DSRC-band application.

1. INTRODUCTION

Since the last decade, the use of vehicular communications has been enhanced due to some challenges in transport systems like traffic congestion, accidents, electronic toll collection, parking, emergency alerts, etc. Such communications stand on wireless communication technology, known as dedicated short-range communication [1]. Therefore, the antenna needed for such applications should be small in size, with a minimum bandwidth of 75.00 MHz around 5.90 GHz [5.850–5.925 GHz], and a uniform radiation pattern with high gain.

Microstrip antennas are widely used for this band of frequencies, as they have advantages like low cost and weight, easy fabrication, low profile, and compactness, which make them suitable for road communications [2–5]. The conventional patch suffers from a low gain and narrow bandwidth. Many techniques have been proposed to improve the gain and bandwidth of patch antennas. The modifications in the patch geometry also improve the performance of the patch [6–13]. A bulky antenna can be made compact by combining fractal geometries in the design. The self-similarity and space-filling nature of the fractal geometries are interconnected to its frequency characteristics, i.e., small size, multiband frequency operation, and symmetricity in radiation pattern. Various geometries such as bow-tie Sierpinski based structure [7] for uniform radiation pattern and high directivity, E-shaped antenna [8] for wide-band applications, Minkowski fractal [10] based geometry for multi-band application, petal shape patch [12] antenna for WLAN/WiMAX application, and hexagon shaped geometric [13] for low-polarized antenna have been reported in the literature. In some cases, the fractal geometry does not accomplish the need of providing the required frequency of operation, which can be compensated by introducing a Defected

Received 7 February 2020, Accepted 9 April 2020, Scheduled 22 April 2020
* Corresponding author: Deven G. Patanvariya (devenpatanvariya@nitgoa.ac.in).
The authors are with the Department of Electronics and Communication Engineering, National Institute of Technology Goa, Goa, India.

Ground Structure (DGS), which also suppresses the cross-polarization of the antenna. In [11], the cross-polarization in the microstrip patch antenna has been optimized by the probe current control.

The gain of the antenna can be further improved by considering an array topology [2, 14]. The main drawbacks of the array are their large size and complex feed network [15–27]. In an array network, power divider is essential to distribute the power with equal amplitude and phase to each element of the array. In [16], the N-way hybrid power divider has been designed for the antenna feed network. In [17], the authors proposed a modified PIFA and its array for MIMO applications. The high-directivity and low-side-lobe antenna array have been presented in [18] and [25], respectively. The antenna arrays are most suitable for the applications which require beam-shaping and beam-steering of the radiation pattern, like in RADAR and satellite communication systems. Many techniques have been presented in literature [22–24] for antenna beam-steering with help of different materials. In [23], the authors introduced the tri-layer strips to continuously steer the direction of the incident light. The optimization of the nonuniform linear array antenna was presented in [26].

In this paper, a Koch-snowflake based fractal antenna and its array have been presented. To operate both the structures at a desired operating frequency and for a uniform radiation pattern, the authors create a defect in the ground plane. The resultant structure resonates at 5.90 GHz and provides 103.14 MHz impedance bandwidth with 64% CP bandwidth and a CP gain of 6.24 dBic. An equivalent lumped model of the single element, in which the antenna acts as a parallel RLC circuit and its feed line as a T/Pi network, has been presented. In order to get the exact frequency of operation and bandwidth from the equivalent model, the T/Pi network has been derived from the nodal Quality Factor (Qn) [15, 27] of the parallel RLC load. The authors introduce an array structure using a uniform power divider for further improvements in gain. The array feed network has been designed using Wilkinson power dividers, which reduce the overall size of the array structure as well as mutual coupling between the elements. The designed antenna array results in circular polarization with sufficient impedance bandwidth, high gain, and stable radiation pattern. The simulated and fabricated results are in close agreement with each other. Moreover, the proposed antenna, as well as the array, suits well for the DSRC systems.

The outline of this paper is as follows. Section 2 describes the proposed antenna geometry along with fractal length calculation and circuit model of the antenna. The antenna array feed network is discussed in Section 3. Results and discussion of simulation as well as measurement results of the prototypes are explained in Section 4. Finally, the conclusions are drawn in Section 5.

2. PROPOSED FRACTAL

The development of fractal geometry and its working has been discussed in detail. Also, the fractal length of the proposed geometry and surface current distribution of the antenna has been explained.

2.1. Fractal Formation

Initially, a square geometry has been considered with a proper dimension, as shown in Figure 1(a). A truncated triangular shape geometry is introduced after implementing the Koch-snowflake first iteration on each side of the initialized square. These truncated squares are then removed from the squared geometry, and as a result, a fractal structure is obtained as shown in Figure 1(b). Here, the reason for taking the 1st iteration of Koch-snowflake on the four sides of the conventional square is for space-filling

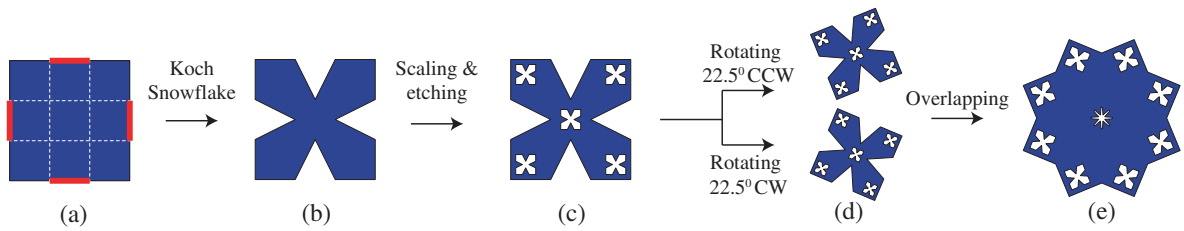

Figure 1. (a)–(e) steps configuration of the proposed fractal geometry.

which stretches the surface current path to resonate the antenna at the desired frequency and reduces the size of the geometry. Also, the perimeters have been increased without boundary. Considering the latest obtained geometry and implementing 83.31% scale of its area, it is placed in all the corners of the Figure 1(b) as well as its center. These five scaled geometries are then subtracted or etched from Figure 1(b) to obtain a revised fractal structure as illustrated in Figure 1(c). The geometry in Figure 1(c) is rotated by 22.50° in counter-clockwise (CCW) as well as clockwise direction (CW), which is depicted in Figure 1(d). The rotation of 22.50° in both the directions has been done for the symmetric structure and to avoid the overlap in the geometry. Both the geometries of Figure 1(d) are then superimposed to each other, to form the proposed fractal geometry, which is shown in Figure 1(e). The rule of thumb for the design is to modify the current path of the antenna in such a manner to resonate the structure at required frequency. Towards that direction, the 1st iteration of Koch-snowflake, which is commonly used to increase the fractal length has been implemented. In order to increase the radiating surface of the antenna and to impose symmetry in the structure, overlap of the two rotated versions of the geometries of Figure 1(d) has been performed.

2.2. The Proposed Structure of Single Element

The proposed fractal geometry is placed on top of the substrate material, Rogers RT Duroid 5880 having $\epsilon_r = 2.20$, and is shown in Figure 2(a) to design a microstrip patch antenna. The width of the radiating element of the antenna is represented by W_P. Inside the proposed geometry, two more slots are implemented, having length C_L and width C_W, to satisfy the circular polarization property of the antenna. The slots are placed at an angle of 45° to the center of the geometry. A stripline feed with a proper dimension L_F is connected with the patch to provide the excitation power. The radiating patch consists of eight flower-shaped etched portions having the dimension W_{cut}.

To resonate the structure at the desired frequency and to have the symmetric radiation pattern, defect on the ground plane has been created as shown in Figure 2(b). The two diagonal slots having the equal-half length of the substrate have been used to create the defects in the ground plane. The slots are placed at an angle of 45° to the center of the layer. Figure 2(c) represents the side-view of the proposed antenna element. The length of the conventional square patch to resonate at 5.90 GHz is 17.14 mm. The side length of the proposed single element is computed equal to 14.38 mm, and hence, the percentage of reduction in the size of the proposed antenna becomes 29.61%. The size reduction has been achieved due to implementation of the Koch-snowflake fractal on the conventional geometry. Also, in the conventional patch, the overall radiating area is 293.77 mm^2 while in the proposed fractal antenna overall radiating area is 175.50 mm^2. Hence, a 40.26% surface area reduction has been achieved after implementing the fractal geometry.

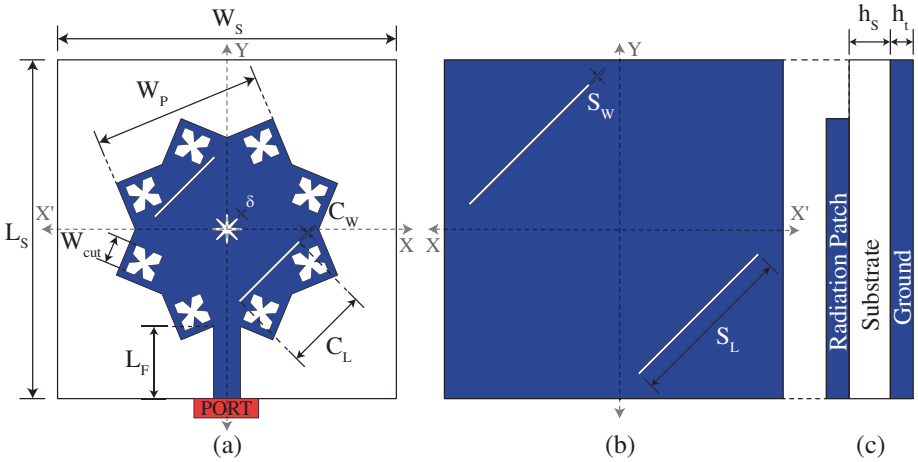

Figure 2. Structure and detailed dimensions of the proposed patch antenna: (a) Top-view. (b) Rear-view. (c) Side-view. $W_S = 28.76$, $L_S = 28.76$, $W_P = 14.38$, $C_W = 0.20$, $C_L = 7.19$, $W_{cut} = 2.40$, $L_F = 6.12$, $S_W = 0.20$, $S_L = 14.38$, $\delta = 0.10$, $h_S = 0.787$ and $h_t = 0.017$ (All dimensions in mm).

2.3. Fractal Length Calculation

A fractal is an object that displays a property known as self-similarity, i.e., a geometric shape that can be reduced to smaller parts, with each smaller part being a reduced copy of the whole [6]. A fractal dimension is a statistical quantity that describes how a fractal appears to fill space. The total fractal length (F) of the proposed geometry of Figure 2(a) is obtained from Equation (1) as:

$$F = (16 \times W_p^1) + \left(\frac{64}{9} \times W_p\right) + (4 \times (C_L + C_W)) + \left(16 \times \left(\frac{W_p}{18} + \delta\right)\right) \tag{1}$$

where $W_p^1 = \frac{W_p}{3.414}$, $W_{cut} = \frac{W_p}{6}$, and $\delta = \frac{W_p}{144}$, so $F = 213.60$ mm. Since the same size of the square without fractal geometry $R = 68.56$ mm is considered, fractal patch length has been increased due to the fractal geometry. Stretching of the current path length has been done in a radiating patch by introducing the fractal approach to reduce the resonant frequency.

2.4. Surface Current

The surface current spreading on the antenna decides the antenna functionality as well as the radiation pattern. Any modification on the geometrical structure of the antenna creates a new current path and radiation, which leads to the new resonating frequency. The surface current distribution has been shown in Figure 3(a). The enlarged portion of a patch in Figure 3(b) reflects a current path in which arrows indicate the current direction on a patch. The proposed design using Koch-snowflake fractal gives the average current path length (C_P) which is given by,

$$C_p = \left(\frac{2}{3} \times W_{cut}\right) + C_W + \frac{C_L}{2} + \frac{W_p}{\sqrt{3}} + \left(\frac{4}{3} \times W_{cut}\right) + \Delta \tag{2}$$

where $\Delta = 0.50$ mm and W_{cut}, C_W, C_L, W_P values are given in Figure 2. From the above equation, the average current path length of the proposed antenna is 17.40 mm, which is the same as a simple square microstrip patch antenna operating at 5.90 GHz. The proposed patch has been simulated by a microstrip feed line having a characteristic impedance of 50 Ω. By using a finite integration based tool 'CST Microwave Studio', the proposed patch is found to be operating at 5.90 GHz.

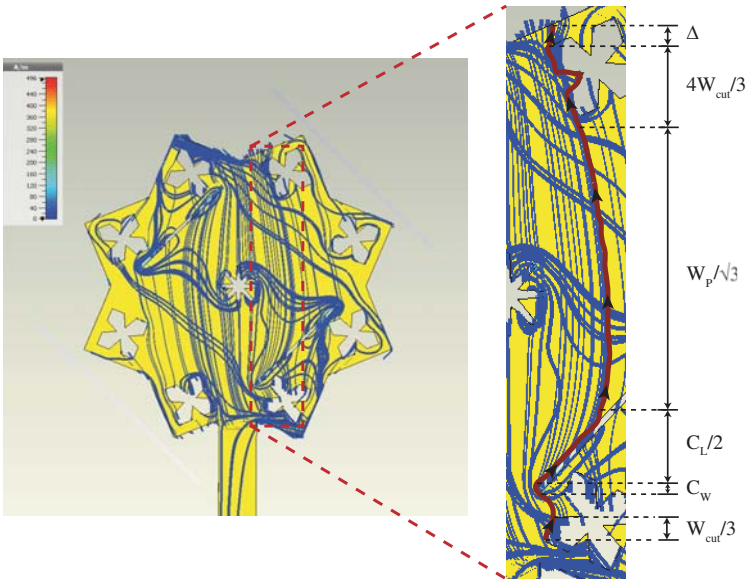

Figure 3. Average current path calculation: (a) Surface current of the patch antenna. (b) Magnification of highlighted square of a current path.

2.5. Circuit Equivalent Model

The circuit model of the proposed patch antenna with feed is shown in Figure 4. The circuit model represents the proposed single element by a parallel combination of resistance (R), inductance (L), and capacitance (C). The values of R, L, and C can be calculated [12, 15] by the following Equations (3)–(6):

$$C = \frac{WL\epsilon_o\epsilon_{eff}}{2h_s} \tag{3}$$

$$R = \frac{Q}{\omega_r C} \tag{4}$$

$$L = \frac{1}{C\omega_r^2} \tag{5}$$

$$Q = \frac{c\sqrt{\epsilon_{eff}}}{\kappa f h} \tag{6}$$

where W and L are the width and length of the proposed patch. ϵ_{eff} is the effective permittivity of the substrate, and κ is a constant. h_s and Q are the height of the substrate and quality factor, respectively. R, L, and C values are listed in Table 1. The characteristic impedance of the transmission line is approximately $50\,\Omega$, and the microstrip feed line length is 0.12λ, which has been obtained using the sweep parameter analysis of CST Microwave Studio. After moving from source to load in Smith chart, the obtained value of Z_L is $(1.22 - j0.042)\Omega$.

Table 1. Parametric value of the lumped equivalent circuit model.

Parameter	Value	Parameter	Value	Parameter	Value
R	$61.00\,\Omega$	$L1$	1.36 nH	$L1'$	1.45 nH
L	0.33 nH	$L2$	1.34 nH	$L2'$	1.45 nH
C	2.22 pF	$C1$	0.47 pF	$C1'$	0.49 pF

The equivalent circuit of the feed is derived by considering T or Pi networks. The reason for choosing T/Pi equivalent network for the feed is to keep a similar type behavior in the S_{11} parameter between the equivalent circuit and the proposed patch antenna [15, 27]. The complete circuit equivalent models of an antenna having a T/Pi network followed by RLC load are shown in Figures 4(a), (b), and (c), respectively. The component values of T/Pi networks are computed from the Smith Chart. All the equivalent circuit models of a single element have been simulated using Cadence.

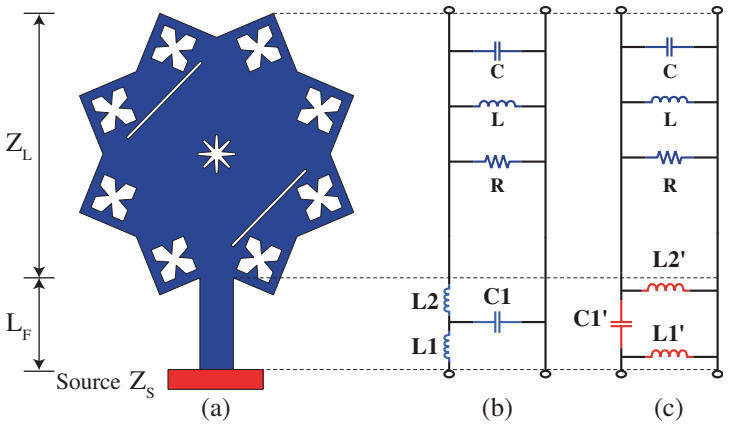

Figure 4. The proposed antenna and its Lumped equivalent model: (a) antenna with feed. (b) T network followed by RLC load. (c) Pi network followed by RLC load.

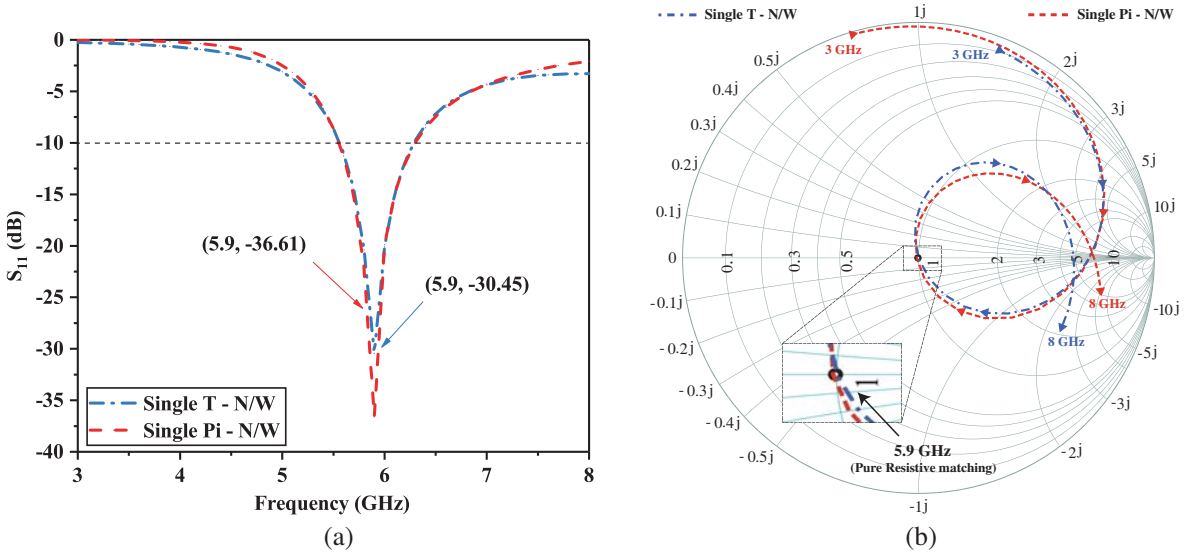

Figure 5. (a) Reflection coefficient of the T and Pi network with antenna as RLC Load. (b) Input impedance response of the T and Pi network with antenna as RLC Load.

The output reflection coefficients of T/Pi networks are shown in Figure 5(a), which indicates an exact resonating frequency of 5.90 GHz with adequate bandwidth and return loss. The effects of fringing fields, dielectric material, ground plane, and mutual coupling effect are neglected in the model. The input impedance response of the circuits is shown in Figure 5(b). The magnifying portion of Figure 5(b) ensures a pure resistive input impedance of 50 Ω from the equivalent circuit at resonating frequency for both T and/or Pi type of matching networks.

3. CONSTRUCTION OF ANTENNA ARRAY

Further radiation patterns and gain of the antenna can be improved with the help of an array topology. The polarization of the radiated wave is one of the most essential characteristics of the antenna. The circularly polarized antenna has become the new eras of the communication systems. For more effective parametric results, the proposed elements are organized in such a way to achieve circular polarization. The inter elements spacing is considered as 0.50λ [2] to reduce the effect of the mutual coupling. Analysis of the feed line loss and port phases is essential while forming the feed structure.

3.1. Design of Array Feed-Network

The feed network plays a significant role in the complete performance of the antenna in realizing the uniform excitation method, obtaining the preferred radiation pattern of the antenna, and in contributing the right-hand circular polarization. Along the x-axis, the proposed Koch-snowflake based antennas are placed to design a four-element linear array, which not only introduces the symmetry in the structure but also helps to radiate the power in the desired direction. The uniform excited feed network has been designed with the help of a Wilkinson power divider. According to Wilkinson equal power divider principle, two types of the transmission line with different impedance values and 100 Ω chip resistor for isolation have to be considered.

The array with the feed network is shown in Figure 6. In Figure 6, the notation L_1 to L_6 indicates the sub-length of the 50 Ω transmission lines, which has been kept as a multiplication of λ. Similarly, the sum of S_1 to S_3 is $\lambda/4$, as it is matched with impedance using $\lambda/4$ transformer. The mutual coupling between the successive elements of the array has been reduced significantly because of the uniform feed network.

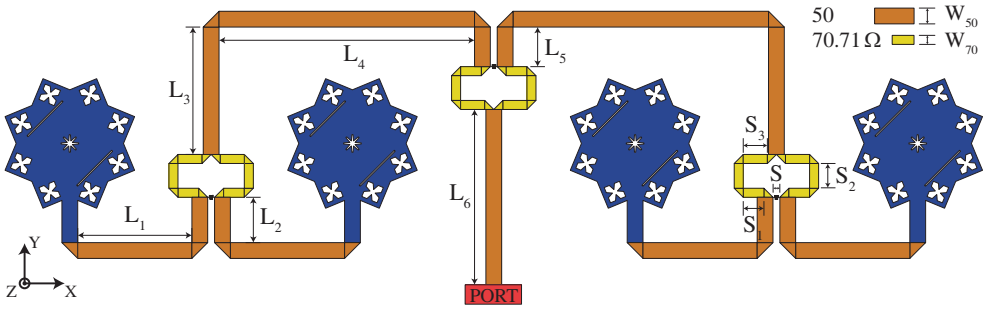

Figure 6. The structure and detailed dimensions of a proposed patch antenna array. $L_1 = 16.60$, $L_2 = 6.57$, $L_3 = 18.47$, $L_4 = 37.05$, $L_5 = 5.74$, $L_6 = 25.42$, $S = 1.00$, $S_1 = 3.00$, $S_2 = 3.60$, $S_3 = 3.50$, $W_{50} = 2.29$ and $W_{70} = 1.31$ (All dimensions in mm).

4. RESULT AND DISCUSSION

The antenna array with the proposed structure has been designed, simulated, and fabricated. The fabricated prototype has been tested and characterized by its main features: return loss, radiation patterns, and polarization. The variations in resonance frequency for different stages of the proposed antenna design are depicted in Figure 7(a). By introducing the 1st iteration of Koch-snowflake, a down-shift in the resonating frequency is obtained. To resonate at the desired frequency of 5.90 GHz, the defect in the ground plane has been created, as shown in Figure 7(a). The parametric study of width variations of top slots and ground slots, in S_{11}, is displayed in Figure 7(b).

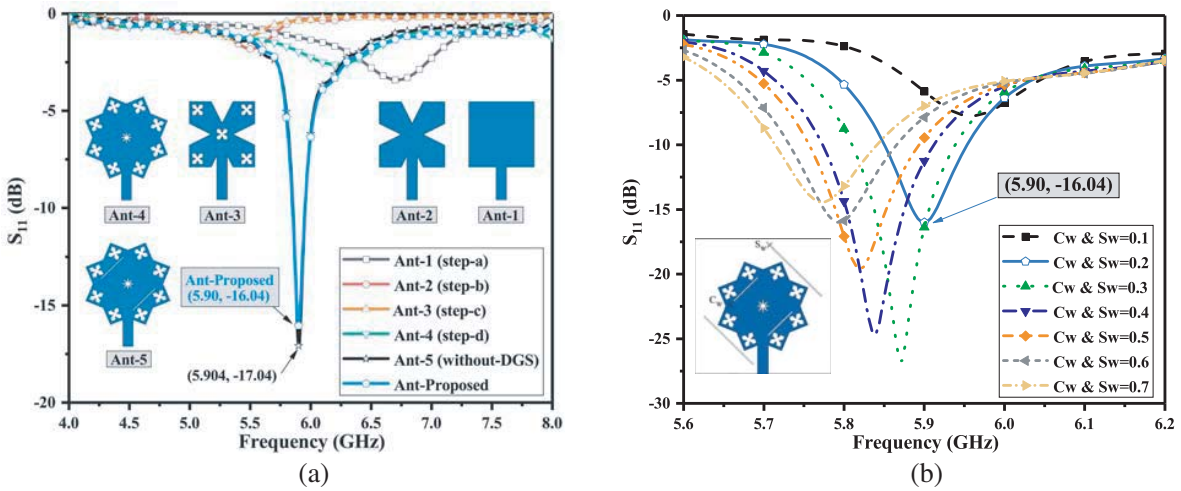

Figure 7. (a) Variations in resonance frequency for different stages of antenna design. (b) Parametric study of the width variations of the rectangular slots.

4.1. Single Element

The fabricated single element top-view and rear-view are shown in Figures 8(a)(i) and (ii), respectively. The measured S-parameters curves are obtained by a 50 Ω one-port Vector Network Analyzer (VNA) N5230A and illustrated in Figure 8(b). The simulated and measured impedance bandwidths of the single element are 103.14 MHz and 115.00 MHz, respectively. A slight deviation in S_{11} is observed, which is due to the mismatch in the fabrication process of the antenna, soldering of SMA connector, and measuring cable of VNA.

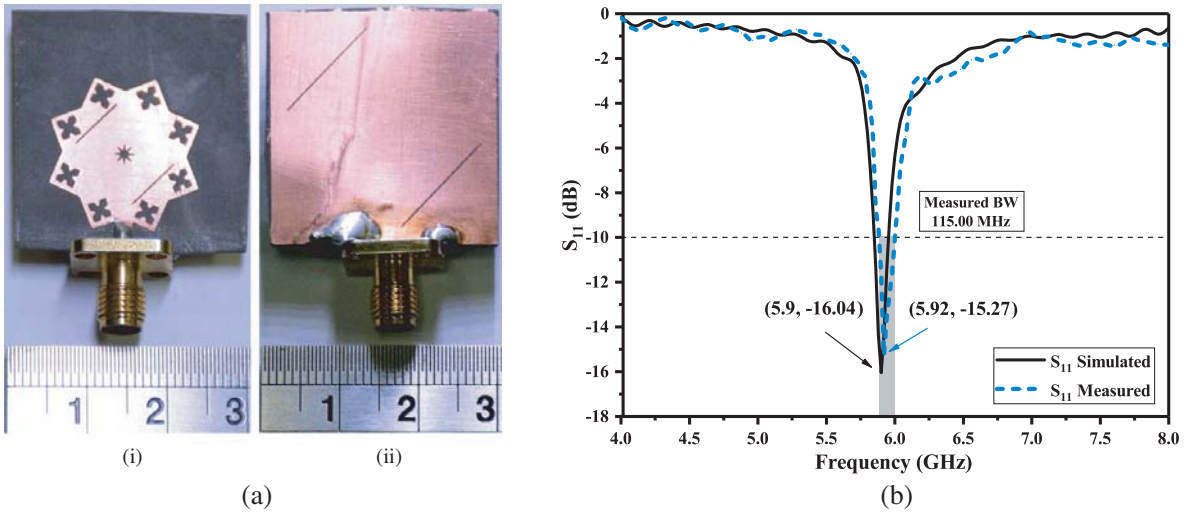

Figure 8. (a) Proposed prototype of single antenna: (i) Top-view. (ii) Rear-view. (b) S_{11} of a single element.

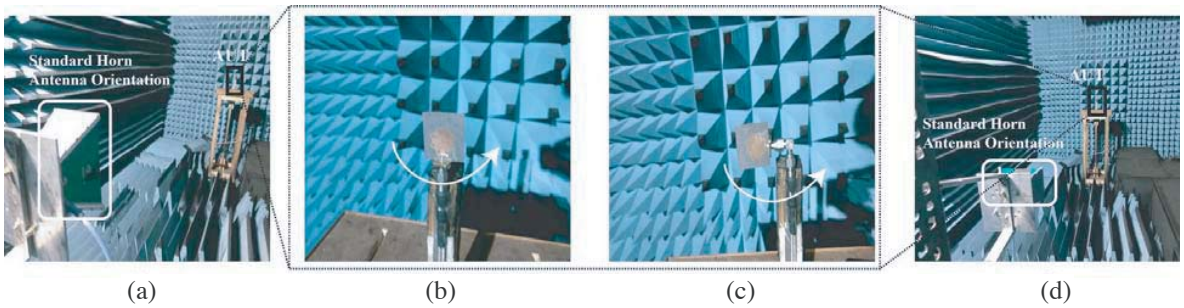

Figure 9. (a)–(d) Photographs of radiation patterns — vertical plane and horizontal plane measurement set-up in an anechoic chamber.

The radiation patterns of the fabricated antennas in both the xz-plane and yz-plane are measured inside an anechoic chamber of Nearfield System Inc. The experimental setup is depicted in Figures 9(a)–(d). To understand and analyze the working mechanism for generating the circular polarization, the distribution and phase of the simulated electric field at 5.90 GHz are illustrated in Figure 10, where the direction of the thin arrow relates to the direction of e-field rotation. It can be observed from Figure 10 that the simulated electric field (E-field) vectors rotate in the counter-clockwise (CCW) direction, which ensures an RHCP in the radiation field of the single element. Figure 11(a) and Figure 11(b) show the comparison between the simulated and measured radiation patterns in xz-plane ($\phi = 0°$) and yz-plane ($\phi = 90°$), respectively. For both planes, the right-hand (RH) circularly polarized fields are stronger than the left-hand (LH) circularly polarized fields, (more than 10 dB), in the boresight direction ($\theta = 0°$). The simulated as well as measured cross-polarization level is more than -13 dB over the entire theta angle in both the planes. The glitches in the pattern arise due to fabrication tolerance and cable loss. The measured Half-Power BeamWidth (HPBW) of the single element is 84.26° in the xz-plane and 85.42° in the yz-plane. The simulated and measured directivities of the proposed antenna are 6.92 dBi and 6.57 dBi, respectively [28].

The parametric performance in terms of axial ratio and RHCP gain of the proposed single element antenna is depicted in Figure 12(a), and both results show a good CP performance. It can be seen that the simulated and measured CP bandwidths of a single element are 66.73 MHz and 49.00 MHz, respectively. The simulated and measured axial ratios of single element at 5.90 GHz are 0.31 dB and 1.25 dB, respectively. Similarly, from Figure 12(a), it is observed that the antenna gives the simulated

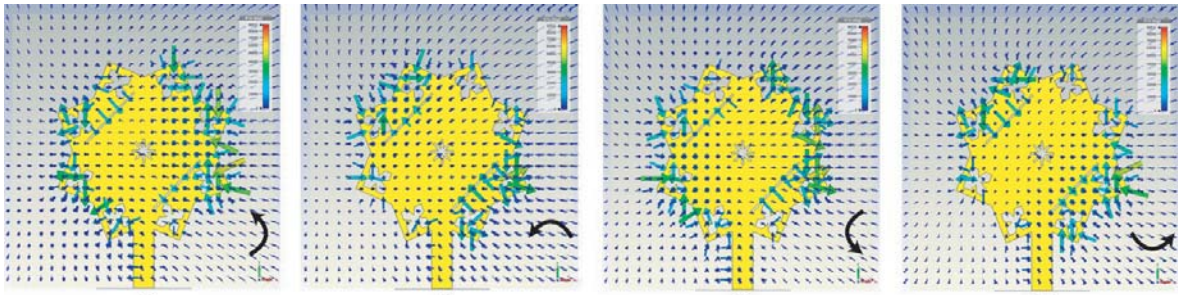

Figure 10. The simulated E-field at 5.90 GHz: (a) 0°, (b) 90°, (c) 180°, (d) 270°.

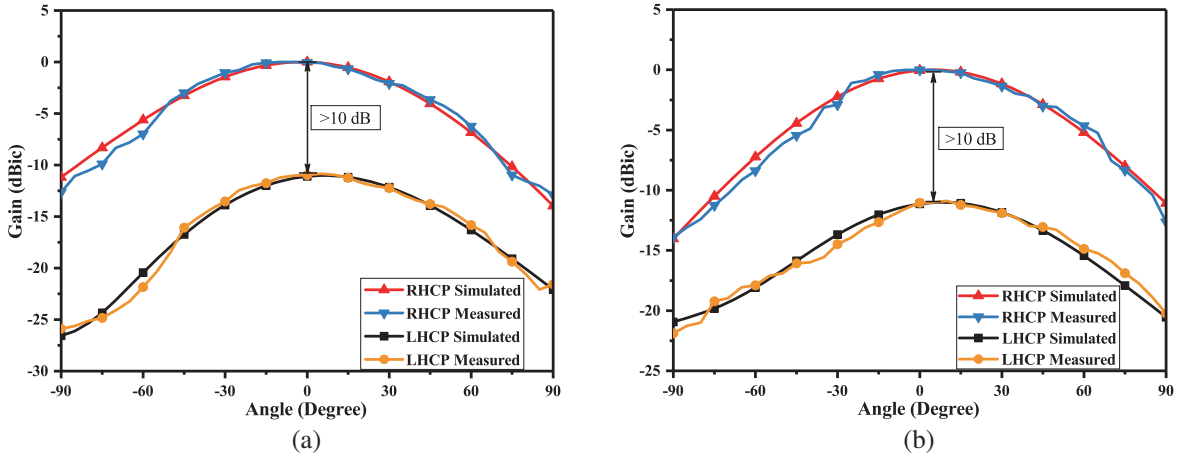

Figure 11. Single element radiation pattern: (a) xz-plane. (b) yz-plane.

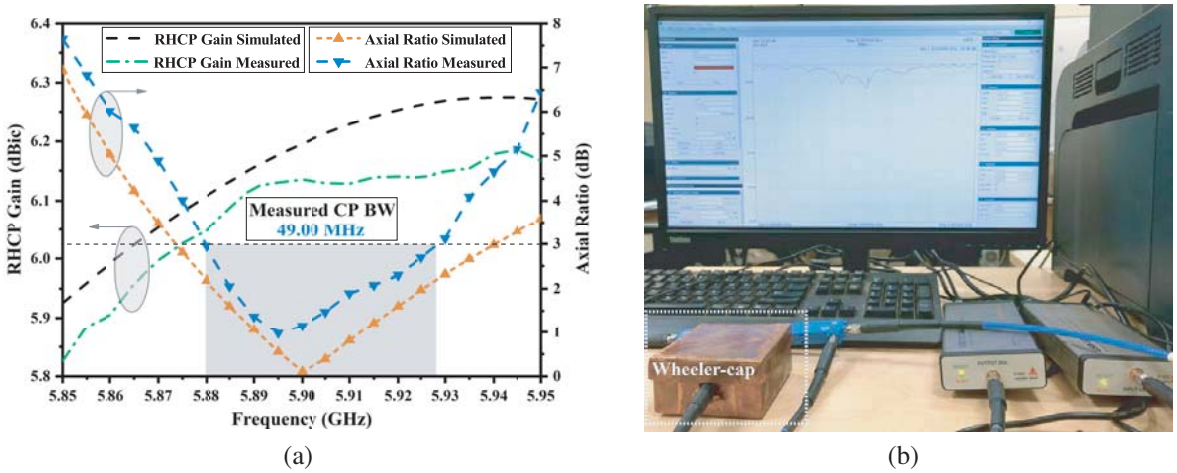

Figure 12. (a) Simulated and measured gain and axial ratio of a single element. (b) Wheeler-cap method of radiation efficiency measurement for a single antenna.

gain 6.24 dBic and measured gain 6.14 dBic at the desired resonating frequency. The gain is calculated by the gain transfer method, where a horn antenna is kept as a reference antenna [28].

The antenna radiation efficiency has been measured with the help of the wheeler cap method [29], whose experimental setup is shown in Figure 12(b). The wheeler cap has been designed using copper plates of thickness 0.56 mm with dimension of $8 \times 8 \times 5\,\text{cm}^3$. The reflection coefficient of the single element with cap is measured from Figure 12(b) and without cap is already recorded from Figure 8(b).

The simulated and measured radiation efficiencies of the proposed single element antenna are 85.47% and 78.17%, respectively.

4.2. Antenna Array

The fabricated prototype array is shown in Figure 13. Figure 14(a) illustrates the simulated and measured S_{11} of the designed antenna array. The simulated and measured impedance bandwidths of array are 108.19 MHz and 165.24 MHz, respectively. The slight discrepancy of the resonant frequency in the fabricated prototype can be due to the fabrication errors, SMA connector, and the effect of commercial substrate variations. However, the achieved bandwidth is sufficient for the DSRC application. Figure 14(b) illustrates the comparison between the branch type feeding network and the proposed feeding network in terms of S_{11}. It can be seen that the branch type feeding network does not resonate.

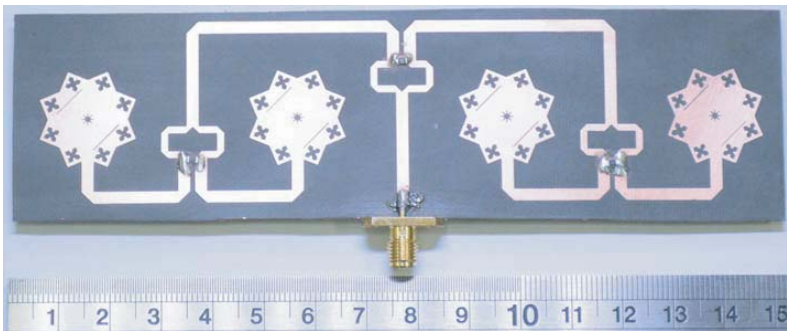

Figure 13. Prototype of antenna array.

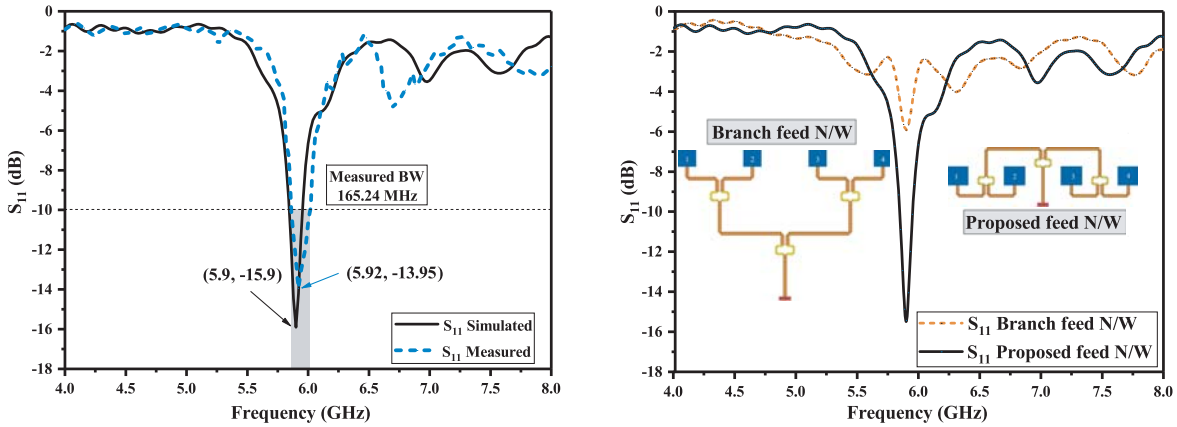

Figure 14. (a) Simulated and measured S_{11} of array. (b) Simulated S_{11} of different array feed.

The comparisons of simulated and measured array gain patterns in two different planes, xz-plane and yz-plane, are shown in Figure 15(a) and Figure 15(b), respectively. The simulated directivity is 13.30 dBi, and VSWR is 1.38, while measured directivity is 12.45 dBi, and derived VSWR is 1.50. The measured HPBW of the array is 18.51° in the xz-plane and 77.45° in the yz-plane, while the SideLobe Level (SLL) is −11.20 dB in xz-plane and −15.08 dB in yz-plane. The simulated and measured cross-polarization level is more than −13 dB over the angular scan range in xz-plane and yz-plane. Similarly, in the array, the simulated E-field vector rotates in the counter-clockwise direction (CCW), which ensures that the proposed array is a right-handed circularly polarized array.

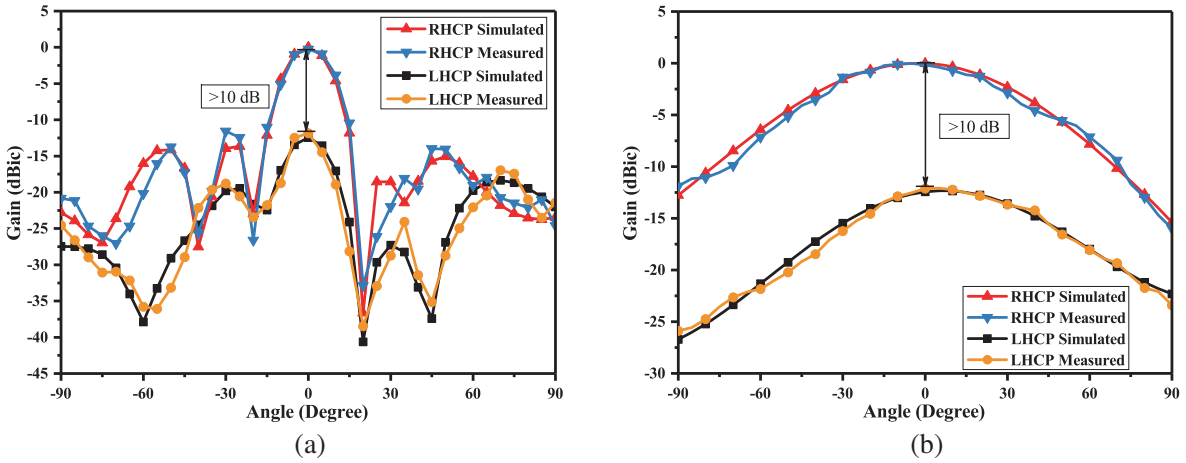

Figure 15. Array radiation pattern: (a) xz-plane. (b) yz-plane.

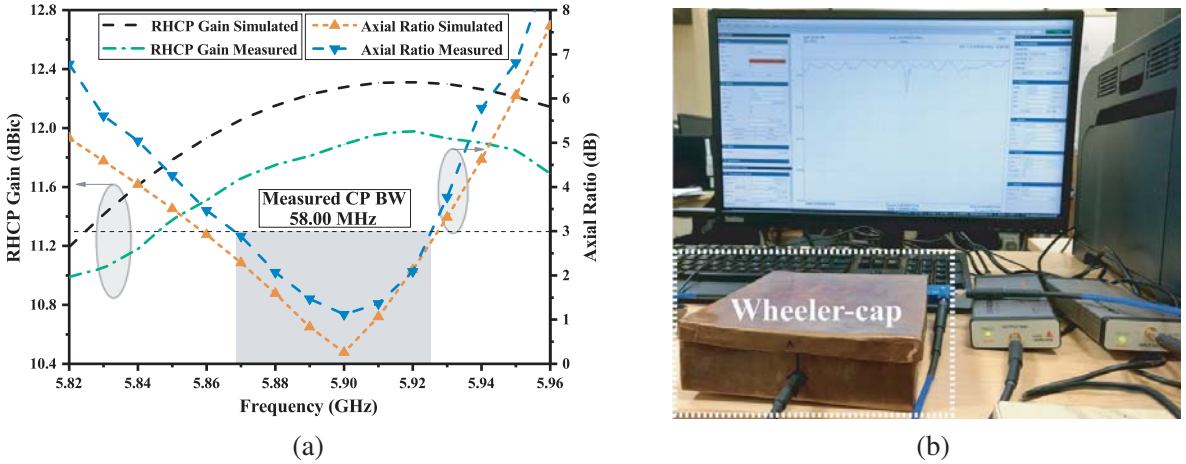

Figure 16. (a) Simulated and measured gain and axial ratio of the array. (b) Wheeler-cap method of radiation efficiency measurement of an antenna array.

The axial ratio and RHCP gain simulated as well as measurement results of the array structure are depicted in Figure 16(a). The simulated and measured axial ratios of an array at 5.90 GHz are 0.38 dB and 1.35 dB, respectively. The simulated and measured CP bandwidths of array are 68.73 MHz and 58.00 MHz, respectively. Similarly, from Figure 16(a), the array gives the simulated RHCP gain 12.30 dBic, and measured gain is 11.98 dBic at the desired resonating frequency.

The experimental setup of radiation efficiency is shown in Figure 16(b). The wheeler box is designed using the same thickness copper plate with the dimensions of $17 \times 17 \times 5\,\text{cm}^3$. Following the same method, the 1st measured reflection coefficient of the array without cap and then measured with cap. The measured radiation efficiency of the array at 5.92 GHz is obtained as 71.50%. Figure 17(a) shows the three-dimensional (3D) gain radiation pattern of the antenna array. The front to back ratio of the single element and array is depicted in Figure 17(b). The value of FBR is grater than 15 dB over the entire resonating band for a single element as well as an array. The mutual coupling influence between the corresponding radiating elements of the array is shown in Figures 18(a) and (b). Figure 18(a) illustrates the mutual coupling between elements without incorporating the feed network while Figure 18(b) represents the mutual coupling after implementing the feed network. The mutual coupling is improved after designing the uniform feed network.

A relative study of the proposed fractal-based antenna and an array in terms of various antenna

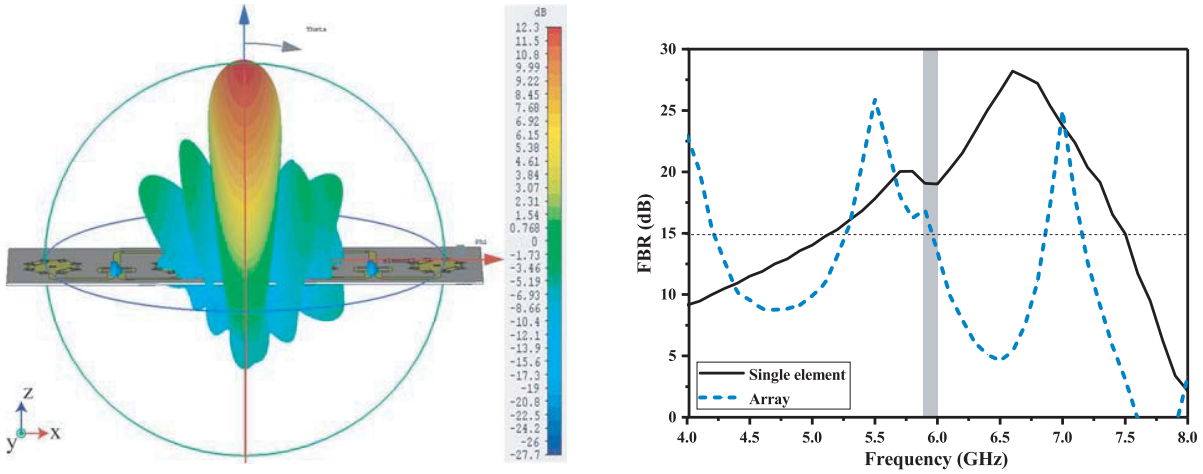

Figure 17. (a) Simulated RHCP 3D gain pattern of the array. (b) Simulated FBR of antenna and array.

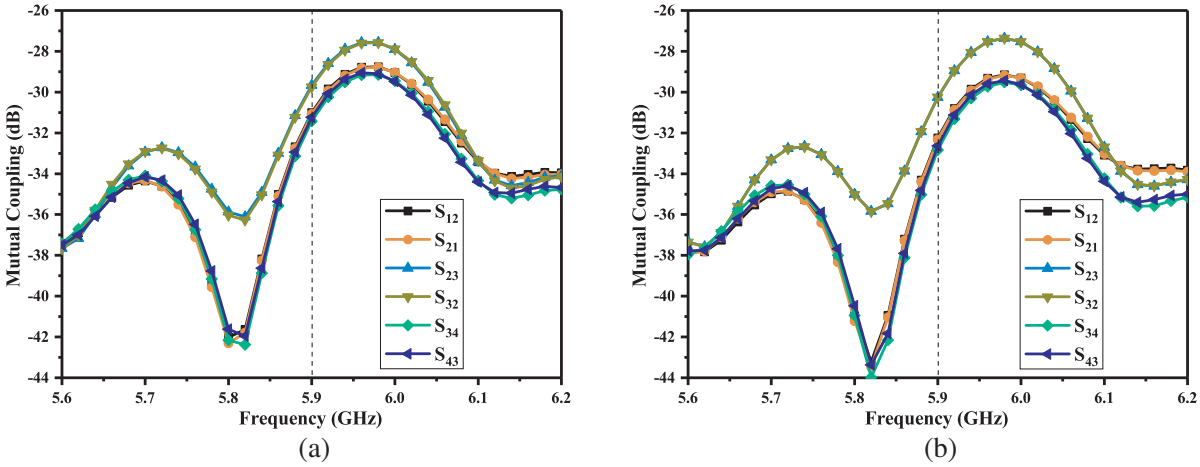

Figure 18. Mutual Coupling: (a) Without feed network. (b) With feed network.

Table 2. Comparative performance of the fabricated prototypes.

Measured Parameters from fabricated prototype	References							
	[8]	[9]	[10]	**Proposed single**	[19]	[20]	[21]	**Proposed Array**
Resonating Frequency [GHz]	5.80	5.20	4.52	**5.92**	5.80	5.90	5.92	**5.92**
Material	Not reported	FR-4	FR-4	**Rogers RT 5880**	FR-4 glass epoxy	Low loss RF laminate	Arlon Cu Clad 217	**Rogers RT 5880**
Dielectric constant	2.20	4.40	4.40	**2.20**	4.60	2.30	4.60	**2.20**
No. of layer	Single layer	Single layer	Single layer	**Single layer**	Single layer	Single layer	Single layer	**Single layer**
S_{11} [dB]	–28.00	–28.00	–22.00	**–15.27**	–20.50	< – 10.00	< – 10.00	**–13.95**
Gain	7.50 dBi	4.50 dBi	1.25 dBi	**6.14 dBic**	11.94 dBi	6.00 dBi	> 6.00 dBi	**11.98 dBic**
Bandwidth [MHz]	830.00	450.00	900.00	**115.00**	325.00	75.00	477.00 Simulated	**165.24**
Radiation efficiency [%]	Not reported	73.00	95.00	**78.17**	Not reported	Not reported	Not reported	**71.50**
RHCP/LHCP	NIL	RHCP	NIL	**RHCP**	NIL	NIL	LHCP	**RHCP**
CP Bandwidth [MHz]	- - -	580.00	- - -	**49.00**	- - -	- - -	316.00	**58.00**
Single/Array element	1	1	1	**1**	8 × 1	4 × 1	4 × 2	**4 × 1**
Size [mm^2]	17.20 × 20	30.00 × 30.00	17.00 × 26.75	**14.38 × 14.38**	- - -	80.00 × 60.00	170.00 × 80.00	**151.70 × 43.50**

parameters are shown in Table 2. It can be observed from Table 2 that the fabricated single element and array give maximum CP gain among all the others. Moreover, the proposed single element and the array are compact in size as shown in Table 2. Therefore, the proposed antennas are suitable for the DSRC band applications.

5. CONCLUSION

This paper presents a uniform linear antenna array, whose performance fulfills the practical specifications of the DSRC band. The antenna is a 4-element array, with a uniform feed network etched on a similar layer to that of the antenna element using equal Wilkinson power divider. A new methodology is introduced in this work by etching the four sides of the square using Koch-snowflake. Also, a defect has been created on the ground plane. Further improvement in parameters has been done by introducing the uniform array. The proposed antenna and the array have been designed and fabricated. The fabricated prototypes reflect an excellent agreement between the simulated and measured results. The proposed single element and the linear array both result in circular polarization. The proposed array gives an impedance bandwidth of 165.24 MHz and CP bandwidth of 58.00 MHz. The presented results make the antennas suitable for short-range communication, such as vehicular to vehicular communication and vehicular to infrastructure communication.

ACKNOWLEDGMENT

This paper is an outcome of the research work undertaken in the project entitled "Design of Compact Shaped Beam Antenna Array for Dedicated Short Range Communication Service" under the SERB Extra Mural Research Funding (File No. SB/S3/EECE/226/2016), Department of Science and Technology, Government of India.

REFERENCES

1. Jiang, D., V. Taliwal, A. Meier, W. Holfelder, and R. Herrtwich, "Design of 5.9 GHz DSRC-based vehicular safety communication," *IEEE Wireless Communications*, Vol. 13, No. 5, 36–43, 2006.
2. Balanis, C. A., *Antenna Theory: Analysis and Design*, John Wiley & Sons, 2016.
3. Pozar, D. M., "Microstrip Antennas," *Proceedings of the IEEE*, Vol. 80, 79–91, 1992.
4. Carver, K. and J. Mink, "Microstrip antenna technology," *IEEE Transactions on Antennas and Propagation*, Vol. 29, No. 1, 2–24, 1981.
5. Guha, D. and Y. M. Antar, Eds., *Microstrip and Printed Antennas: New Trends, Techniques and Applications*, John Wiley & Sons, 2011.
6. Mandelbrot, B. B., *The Fractal Geometry of Nature*, WH freeman, New York, 1983.
7. Anguera, J., C. Puente, C. Borja, R. Montero, and J. Soler, "Small and high-directivity bow-tie patch antenna based on the Sierpinski fractal," *Microwave and Optical Technology Letters*, Vol. 31, No. 3, 239–241, 2001.
8. Ang, B. K. and B. K. Chung, "A wideband E-shaped microstrip patch antenna for 5–6 GHz wireless communications," *Progress In Electromagnetics Research*, Vol. 75, 397–407, 2007.
9. Singh, N., B. K. Kanaujia, M. Tariq Beg, Mainuddin and S. Kumar, "A triple band circularly polarized rectenna for RF energy harvesting," *Electromagnetics*, Vol. 39, No. 7, 481–490, 2019.
10. Banerjee, J., A. Karmakar, R. Ghatak, and D. R. Poddar, "Compact CPW-fed UWB MIMO antenna with a novel modified Minkowski fractal defected ground structure (DGS) for high isolation and triple band-notch characteristic," *Journal of electromagnetic Waves and Applications*, Vol. 31, No. 15, 1550–1565, 2017.
11. Sarkar, C., D. Guha, C. Kumar, and Y. M. Antar, "New insight and design strategy to optimize cross-polarized radiations of microstrip patch over full bandwidth by probe current control," *IEEE Transactions on Antennas and Propagation*, Vol. 66, No. 8, 3902–3909, 2018.

12. Mishra, B., V. Singh, and R. Singh, "Gap coupled dual-band petal shape patch antenna for WLAN/WiMAX applications," *Advances in Electrical and Electronic Engineering*, Vol. 16, No. 2, 185–198, 2018.
13. Joshi, A. and R. Singhal, "Vertex-fed Hexagonal antenna with low cross-polarization levels," *Advances in Electrical and Electronic Engineering*, Vol. 17, No. 2, 138-45, 2019.
14. Haupt, R. L., *Antenna Arrays. A Computational Approach*, 2010.
15. Ludwig, R., *RF Circuit Design: Theory & Applications*, 2 Edition, Pearson Education, India, 2000.
16. Wilkinson, E. J., "An N-way hybrid power divider," *IRE Transactions on Microwave Theory and Techniques*, Vol. 8, No. 1, 116–118, 1960.
17. Gao, Y., C. C. Chiau, X. Chen, and C. G. Parini, "Modified PIFA and its array for MIMO terminals," *IEE Proceedings — Microwaves, Antennas and Propagation*, Vol. 152, No. 4, 255–259, 2005.
18. Jayasinghe, J. M. J. W., J. Anguera, D. N. Uduwawala, and A. Andjar, "High-directivity genetic microstrip patch antenna," *International Journal of Electronics Letters*, Vol. 4, No. 3, 279–286, 2016.
19. Ali, M. T., M. R. Kamarudin, T. B. A. Rahman, R. Sauleau, and M. N. Md Tan, "Design of reconfigurable multiple elements microstrip rectangular linear array antenna," *Progress In Electromagnetics Research C*, Vol. 6, 21–35, 2009.
20. Liu, F., Z. Zhang, W. Chen, Z. Feng, and M. F. Iskander, "An endfire beam-switchable antenna array used in vehicular environment," *IEEE Antennas and Wireless Propagation Letters*, Vol. 9, 195–198, 2010.
21. Varum, T., J. Matos, P. Pinho, R. Abreu, A. Oliveira, and J. Lopes, "Microstrip antenna array for multiband dedicated short range communication systems," *Microwave and Optical Technology Letters*, Vol. 53, No. 12, 2794–2796, 2011.
22. Cao, T., Y. Zou, A. M. Adawi, and M. J. Cryan, "Directive emission of red conjugated polymer embedded within zero index metamaterials," *Optics Express*, Vol. 22, No. 19, 22699–706, 2014.
23. Cao, T., G. Zheng, and S. Wang, "Chemical control of continuous light-steering using an array of gradient Au/Bi_2Se_3/Au strips," *RSC Advances*, Vol. 5, No. 85, 69319-24, 2015.
24. Cao, T., G. Zheng, S. Wang, and C. Wei, "Ultrafast beam steering using gradient Au-$Ge_2Sb_2Te_5$-Au plasmonic resonators," *Optics Express*, Vol. 23, No. 14, 18029-39, 2015.
25. Chatterjee, A., T. Mondal, D. G. Patanvariya, and R. P. K. Jagannath, "Fractal-based design and fabrication of low-sidelobe antenna array," *AEU-International Journal of Electronics and Communications*, Vol. 83, 549–557, 2018.
26. Tran, X. L., J. Vesely, and F. Dvorak, "Optimization of nonuniform linear antenna array topology," *Advances in Electrical and Electronic Engineering*, Vol. 16, No. 3, 341–349, 2018.
27. Patanvariya, D. G., A. Chatterjee, K. Kola, and S. Naik, "Design of a linear array of fractal antennas with high directivity and low cross-polarization for dedicated short range communication application," *International Journal of RF and Microwave Computer-Aided Engineering*, e 22083, 2019.
28. Toh, B. Y., R. Cahill, and V. F. Fusco, "Understanding and measuring circular polarization," *IEEE Transactions on Education*, Vol. 46, No. 3, 313–318, 2003.
29. Moharram, M. A. and A. A. Kishk, "MIMO antennas efficiency measurement using wheeler caps," *IEEE Transactions on Antennas and Propagation*, Vol. 64, No. 3, 1115–1120, 2015.